

# Analytical Performance Evaluation of THz Wireless Fiber Extenders

Alexandros–Apostolos A. Boulogeorgos, Evangelos N. Papatotiriou, and Angeliki Alexiou  
*Department of Digital Systems, University of Piraeus, Piraeus, Greece*  
al.boulogeorgos@ieee.org, {vangpapasot, alexiou}@unipi.gr

**Abstract**—This paper presents the theoretical framework for the performance evaluation of terahertz (THz) wireless fiber extender in the presence of misalignment and multipath fading. In more detail, after providing the appropriate system model that incorporates the different operation, design, and environmental parameters, such as the operation frequency, transceivers antenna gains, the level of misalignment as well as the stochastic behavior of the channel, we extract novel closed-form expressions for the ergodic capacity. These expressions are expected to be used as useful tools for the analysis and design of such systems. Moreover, several insightful scenarios are simulated. Their results highlight the importance of taking into account the impact of misalignment fading when analyzing the performance of the THz wireless fiber extender.

**Index Terms**—Ergodic capacity, Misalignment fading, Performance analysis, Wireless terahertz fiber extender,  $\alpha$ - $\mu$  fading.

## I. INTRODUCTION

Terahertz (THz) fiber extenders have received considerable attention due to the unprecedented increase in the bandwidth and ultra-high data rates that they offer in a cost-efficient and easy deployment manner [2]–[4] as well as the fact that they can contribute to bridging the connectivity gaps that exist between the radio frequency (RF) access network and the fiber optic based backbone network [2]. This application scenario is expected to be employed in developing countries, where there may not be much of a fiber optic structure and hence to increase its reach and bandwidth to the last mile, without requiring a huge amount of economic resources to dig up the current brown-field [5], [6].

However, THz systems are subject to high path losses [4], [7], which originate from the band’s high frequencies that cause interaction and energy absorptions by the molecules of the propagation medium [8]. To understand the nature of these absorptions and to design countermeasures, a great amount of effort was put in modeling the THz channel particularities [9], evaluating their impact on the system’s performance [10] and proposing countermeasures [11]–[13]. In particular, the THz channel characteristics were studied in several

works including [14]–[19] and references therein. In more detail, in [14], the authors presented a novel propagation model for THz nano-scale communications. Additionally, in [15], a simplified path-loss model for the 275 – 400 GHz band was introduced. Furthermore, in [16], a multi-ray THz propagation model was presented, while, in [17], a propagation model for intra-body nano-scale communications was provided. Likewise, in [18], a path-loss model, which quantifies the total absorption loss assuming that air, natural gas and/or water are the components of the propagation medium, was reported, whereas, in [19], a multi-ray THz propagation model was presented.

Although all the above contributions revealed the particularities of the THz medium, they neglected the impact of fading, which can be generated due to scattering on aerosols in the atmosphere [20]. On the contrary, in [21]–[24], the authors presented suitable stochastic models that are able to accommodate the multipath fading effect in the THz band. In particular, in [21], the authors introduced a multi-path THz channel model, where the attenuation factor was modeled as a Rayleigh or Nakagami- $m$  distributions under the non-line-of-sight condition and as a Rician or Nakagami- $m$  distribution under the line-of-sight assumption. Moreover, in [22] and [23], the authors assumed Rician fading to accommodate the stochastic characteristics of the THz communication channel. Likewise, in [24], the authors used a log-normal shadowing path-loss model for THz nano-sensor communications.

It is also widely known that another characteristic of THz systems that may cause severe performance degradation is the misalignment between the transmitter (TX) and receiver (RX) antennas beams. The impact of TX-RX beams misalignment in the THz link was discussed in [21], [23] and [25]. In more detail, in [21] and [25], the authors assumed deterministic models to incorporate the impact of antennas’ misalignment, while, in [23], it was considered to be a part of the shadowing effect. The disadvantage of these models is that they are unable to accommodate the stochastic characteristics of phenomena such as thermal expansion, dynamic wind loads and weak earthquakes, which result in the sway of high-rise buildings and cause vibrations

This work has received funding from the European Commissions Horizon 2020 research and innovation programme under grant agreement No. 761794.

This paper is the conference version of the paper [1], which includes new insightful results.

of the transceivers antennas; in other words, the effect of misalignment between the TX and RX [26].

To the best of the authors' knowledge, the effect of misalignment over fading channel in the THz band has not been addressed in the open literature. Motivated by this, this paper is focused on providing the theoretical framework for the quantification of the performance of THz wireless fiber extenders. In particular, the technical contribution of this paper is outlined below:

- We establish an appropriate system for the THz wireless fiber extenders, which takes into account the different design parameters, the channel characteristics, as well as their interactions. These parameters include the transmission range, the TX and RX antennas' gains, the degree of TX and RX misalignment, the transmission and noise power.
- In order to analytically evaluate the performance of the THz wireless extender, we extract novel closed-form expressions for the ergodic capacity.

*Notations:* The operators  $\mathbb{E}[\cdot]$  and  $|\cdot|$  respectively denote the statistical expectation and the absolute value, whereas  $\exp(x)$  and  $\log_2(x)$  stand for the exponential function and the logarithmic function with base 2. Additionally, the operator  $\ln(x)$  refers to the natural logarithm of  $x$ , while, the operator  $\sqrt{x}$  returns the square root of  $x$ . Likewise, the set of the complex numbers is represented by  $\mathbb{C}$ , while  $CN(x, y)$  denotes a  $x$ -mean complex Gaussian process with variance  $y$ . The upper and lower incomplete Gamma functions [27, eq. (8.350/2), (8.350/3)] are respectively denoted by  $\Gamma(\cdot, \cdot)$  and  $\gamma(\cdot, \cdot)$ , while the Gamma function is represented by  $\Gamma(\cdot)$  [27, eq. (8.310)]. Finally,  ${}_2F_1(\cdot, \cdot; \cdot; \cdot)$  and  $G_{p,q}^{m,n} \left( x \left| \begin{matrix} a_1, a_2, \dots, a_p \\ b_1, b_2, \dots, b_q \end{matrix} \right. \right)$  respectively stand for the Gauss hypergeometric function [28, eq. (4.1.1)] and the Meijer's G-function [27, eq. (9.301)], whereas  $H_{p,q}^{m,n} \left[ z \left| \begin{matrix} (a_1, b_1), \dots, (a_p, b_p) \\ (c_1, d_1), \dots, (c_p, d_p) \end{matrix} \right. \right]$  is the Fox H-function [29, eq. (8.3.1/1)].

## II. SYSTEM & CHANNEL MODEL

As depicted in Fig. 1.a, we consider a THz wireless fiber extender, in which the TX and RX are equipped with highly directive antennas. The information signal,  $x \in \mathbb{C}$ , is conveyed over a flat fading wireless channel  $h \in \mathbb{C}$  with additive noise  $n \in \mathbb{C}$ . Therefore, the baseband equivalent received signal can be expressed as

$$y = hx + n, \quad (1)$$

where  $h$ ,  $x$  and  $n$  are statistically independent. Likewise,  $n$  is modeled as a complex zero-mean additive white Gaussian process with variance equals  $N_o$ .

The channel coefficient,  $h$ , can be obtained as

$$h = h_l h_p h_f, \quad (2)$$

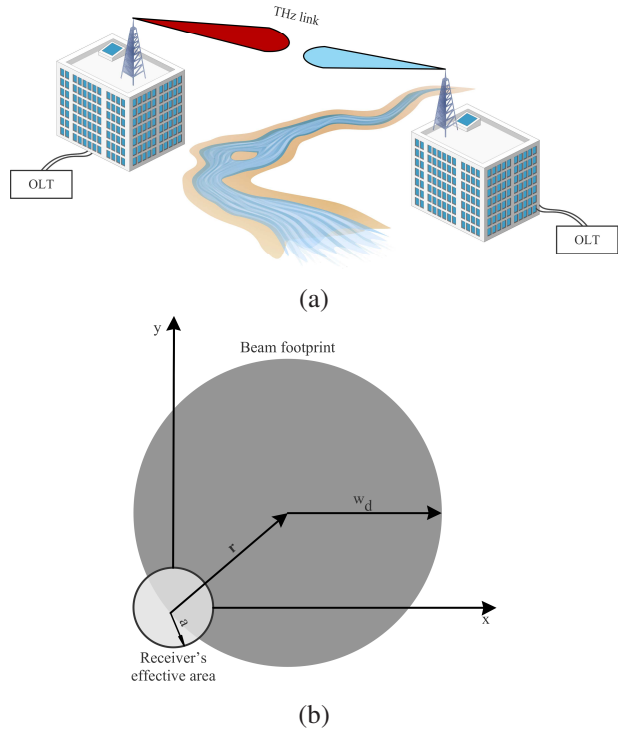


Fig. 1: (a) System model. OLT stands for the optical line terminal. (b) RX's effective area and TX's beam footprint with misalignment on the RX's plane.

where  $h_l$ ,  $h_p$  and  $h_f$  respectively model the deterministic path gain, the misalignment fading, which results in pointing errors, and the stochastic path gain.

The deterministic path gain coefficient can be expressed as  $h_l = h_{fl} h_{al}$ , where  $h_{fl}$  models the propagation gain and can be written as  $h_{fl} = \frac{c\sqrt{G_t G_r}}{4\pi f d}$ , where  $G_t$  and  $G_r$  respectively represent the antenna orientation dependent transmission and reception gains,  $c$  stands for the speed of light,  $f$  is the operating frequency and  $d$  is the distance between the TX and the RX. Additionally,  $h_{al}$  denotes the molecular absorption gain and can be evaluated as  $h_{al} = \exp(-\frac{1}{2}\kappa_\alpha(f)d)$ , where  $\kappa_\alpha(f)$  denotes the absorption coefficient that describes the relative area per unit of volume, in which the molecules of the medium are capable of absorbing the electromagnetic wave energy, and can be evaluated as [15].

As demonstrated in Fig. 1.b, we assume that the RX has a circular detection beam of radius  $\alpha$ , covering an area  $A$ . Moreover, the TX has also a circular beam, which at distance  $d$  has a radius  $\rho$  that belongs in the interval  $0 \leq \rho \leq w_d$ , where  $w_d$  is the maximum radius of the beam at distance  $d$ . Furthermore, both beams are considered on the positive Cartesian  $x-y$  plane and  $r$  is the pointing error expressed as the radial distance of the transmission and reception beams. Due to the symmetry of the beam shapes,  $h_p$  depends only on the radial

distance  $r = |r|$ . Therefore, without loss of generality, it is assumed that the radial distance is located along the  $x$  axis. As a consequence and according to [30], the misalignment fading coefficient,  $h_p$ , which represents the fraction of the power collected by the RX, covering an area  $A$  at distance  $d$  can be approximated as

$$h_p(r; d) \approx A_o \exp\left(-\frac{2r^2}{w_{deq}^2}\right), \quad (3)$$

where  $w_{deq}$  is the equivalent beam-width, whereas  $A_o$  is the fraction of the collected power at  $r = 0$  and can be calculated as  $u = \frac{\sqrt{\pi}a}{\sqrt{2}w_d}$ , with  $a$  being the radius of the RX effective area and  $w_d$  is the radius of the TX beam footprint at distance  $d$ . Additionally, the equivalent beam-width,  $w_{eq}^2$ , is related to  $w_d^2$  through  $w_{eq}^2 = w_d^2 \frac{\sqrt{\pi} \operatorname{erf}(u)}{2u \exp(-u^2)}$ .

By considering independent identical Gaussian distributions for the elevation and horizontal displacement [30], [31], the radial displacement at the RX follows a Rayleigh distribution with probability density function (PDF), which can be expressed as

$$f_r(r) = \frac{r}{\sigma_s^2} \exp\left(-\frac{r^2}{2\sigma_s^2}\right), \quad (4)$$

where  $\sigma_s^2$  is the variance of the pointing error displacement at the RX. By combining (3) and (4), the PDF of  $|h_p|$  can be expressed as [30]

$$f_{h_p}(x) = \frac{\xi}{A_o^\xi} x^{\xi-1}, \quad 0 \leq x \leq A_o, \quad (5)$$

where  $\xi = \sqrt{\frac{w_{eq}}{2\sigma_s}}$  is the ratio between the equivalent beam width radius at the RX. Note that this model was extensively used in several studies in free space optical systems (see e.g., [32], [33] and references therein).

The stochastic path gain coefficient,  $|h_f|$ , is assumed to follow an  $\alpha - \mu$  distribution [34], with PDF given by

$$f_{h_f}(x) = \frac{\alpha\mu^\mu}{\hat{h}_f^{\alpha\mu} \Gamma(\mu)} x^{\alpha\mu-1} \exp\left(-\mu \frac{x^\alpha}{\hat{h}_f}\right), \quad (6)$$

where  $\alpha > 0$  is a fading parameter,  $\mu$  is the normalized variance of the fading channel envelope, and  $\hat{h}_f$  is the  $\alpha$ -root mean value of the fading channel envelop. Note that this distribution is a general form for many well-known distributions, such as Rayleigh ( $\alpha = 2, \mu = 1$ ), Nakagami- $m$  ( $\alpha = 2$  and  $\mu$  is the fading parameter), Weibull ( $\mu = 1$  and  $\alpha$  is the fading parameter), etc. [35].

### III. PERFORMANCE ANALYSIS

Theorem 1 returns a novel closed-form expression for the evaluation of the ergodic capacity.

**Theorem 1.** *The ergodic capacity can be analytically expressed as in (7), given at the top of the next page. In (7),  $\Delta = \frac{|h_i|^2 P}{N_o}$ ,  $\Lambda = \xi - 1$ ,  $\Phi = \frac{\alpha\mu - \xi}{\alpha}$ ,  $X = \frac{\mu}{\hat{h}_f^\alpha A_o^\alpha}$*

$$\text{and } \Theta = \xi A_o^{-\xi} \frac{\mu^{\mu - \frac{\mu\alpha - \xi}{\alpha}}}{\hat{h}_f^\alpha \Gamma(\mu)}.$$

*Proof:* Based on (1), the instantaneous SNR of the received signal can be obtained as

$$\gamma = \frac{|h|^2 P}{N_o}. \quad (8)$$

Hence, the ergodic capacity can be defined as  $C = \mathbb{E}[\log_2(1 + \gamma_i)]$ , or

$$C = \mathbb{E}[\log_2(1 + \Delta|h_{fp}|^2)], \quad (9)$$

which can be evaluated as

$$C = \int_0^\infty \log_2(1 + \Delta x^2) f_{|h_{fp}|}(x) dx, \quad (10)$$

where  $f_{|h_{fp}|}(x)$  stands for the probability density function of the random variable  $h_{fp} = h_f h_p$  and can be evaluated, according to [36], as

$$f_{|h_{fp}|}(x) = \int_0^{A_o} \frac{1}{y} f_{|h_f|}\left(\frac{x}{y}\right) f_{|h_m|}(y) dy. \quad (11)$$

By substituting (5) and (6) into (11), the PDF of  $|h_{fp}|$  can be equivalently expressed as

$$f_{|h_{fp}|}(x) = \frac{\alpha\mu^\mu x^{\alpha\mu-1}}{(\hat{h}_f)^\alpha \Gamma(\mu)} \frac{\xi}{A_o^\xi} \mathcal{I}(x), \quad (12)$$

where

$$\mathcal{I}(x) = \int_0^{A_o} y^{\xi-\alpha\mu-1} \exp\left(-\mu \frac{x^\alpha y^{-\alpha}}{\hat{h}_f}\right) dy. \quad (13)$$

By employing [27, eq. (8/350/1)], (12) can be written as

$$f_{|h_{fp}|}(x) = \xi A_o^{-\xi} \frac{\mu^\xi}{\hat{h}_f^\alpha \Gamma(\mu)} x^{\xi-1} \times \Gamma\left(\frac{\alpha\mu - \xi}{\alpha}, \mu \frac{x^\alpha}{\hat{h}_f} A_o^{-\alpha}\right). \quad (14)$$

Next, by substituting (14) into (10), the ergodic capacity can be expressed as

$$C = \frac{\Theta}{\ln(2)} \int_0^\infty x^\Lambda \ln(1 + \Delta x^2) \Gamma(\Phi, X x^\alpha) dx, \quad (15)$$

or, by using [28, eq. (15.1.1)], as

$$C = \frac{\Theta}{\ln(2)} \int_0^\infty x^{\Lambda+1} {}_2F_1(1, 1; 2; -x) \Gamma(\Phi, X x^\alpha) dx. \quad (16)$$

Moreover, by employing [37, eq. (11)] and [27, eq. (9.34/7)], (16) can be written as

$$C = \frac{\Theta}{\ln(2)} \int_0^\infty x^\Lambda G_{2,2}^{1,2}\left(\Delta x^2 \left| \begin{matrix} 1, 1 \\ 1, 0 \end{matrix} \right.\right) \times G_{1,2}^{2,0}\left(X x^\alpha \left| \begin{matrix} 1 \\ 0, \Phi \end{matrix} \right.\right) dx, \quad (17)$$

$$C = \frac{\Theta \Delta^{-\frac{\Lambda+1}{2}}}{\ln(2)} H_{3,4}^{4,1} \left[ \frac{X}{\Delta^{\frac{\alpha}{2}}} \middle| \begin{matrix} (-\frac{\Lambda+1}{2}, \frac{\alpha}{2}), (1 - \frac{\Lambda+1}{2}, \frac{\alpha}{2}), (1, 1) \\ (0, 1), (\Phi, 1), (-\frac{\Lambda+1}{2}, \frac{\alpha}{2}), (-\frac{\Lambda+1}{2}, \frac{\alpha}{2}) \end{matrix} \right] \quad (7)$$

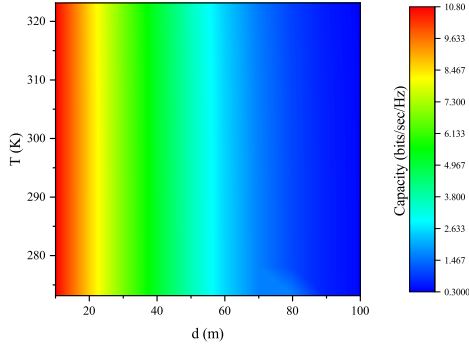


Fig. 2: Capacity vs distance and Temperature, for  $f = 300$  GHz,  $\frac{P}{N_o} = 25$  dB,  $\sigma_s = 0.01$  m

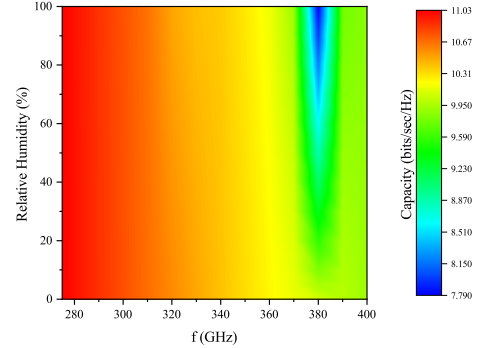


Fig. 3: Capacity vs frequency and relative humidity, for  $d = 10$  m,  $\frac{P}{N_o} = 25$  dB,  $\sigma_s = 0.01$  m.

which, by setting  $z = x^2$ , can be expressed as

$$C = \frac{\Theta}{\ln(2)} \int_0^\infty x^{\frac{\Lambda+1}{2}-1} G_{2,2}^{1,2} \left( \Delta z \middle| \begin{matrix} 1, 1 \\ 1, 0 \end{matrix} \right) \times G_{1,2}^{2,0} \left( X x^{\frac{\alpha}{2}} \middle| \begin{matrix} 1 \\ 0, \Phi \end{matrix} \right) dz. \quad (18)$$

Finally, by using [38] into (18), the ergodic capacity can be rewritten as (7). This concludes the proof. ■

#### IV. RESULTS AND DISCUSSION

In this section, we present the joint effect of the deterministic and stochastic path-gain, i.e., misalignment and multipath fading, components in the ergodic capacity of the THz wireless fiber extender by illustrating analytical and simulation results. Unless otherwise is stated, it is assumed that  $G_t = G_r = 55$  dB<sup>1</sup>,  $\alpha = 2$ , and  $\mu = 4$ . Moreover, standard environmental conditions, i.e.,  $\phi = 50\%$ ,  $p = 101325$  Pa, and  $T = 296$  °K, are assumed. Finally, note that all the analytical results were verified via respective Monte-Carlo simulations.

Fig. 2 shows the ergodic capacity as a function of the transmission range and atmospheric temperature, assuming  $f = 300$  GHz,  $\frac{P}{N_o} = 25$  dB and  $\sigma_s = 0.01$  m. We observe that, for a fixed temperature, as the transmission range increases, the deterministic path-loss also increases; hence, the ergodic capacity decreases. Similarly, for a given transmission range, as the temperature increases, the molecular absorption loss also increases; therefore, the ergodic capacity degrades. Finally, it is evident that the impact of propagation loss is more severe compared to the one of the molecular absorption, since the ergodic capacity degradation due to a transmission distance increase is considerably more

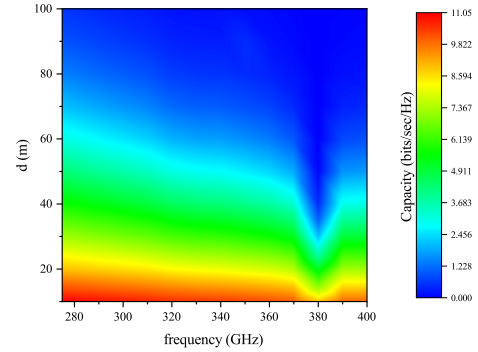


Fig. 4: Capacity vs frequency and distance,  $\frac{P}{N_o} = 25$  dB and  $\sigma_s = 0.01$  m.

detrimental than the corresponding degradation due to a temperature increase.

Fig. 3 demonstrates the ergodic capacity as a function of frequency and relative humidity, assuming  $d = 10$  m,  $\frac{P}{N_o} = 25$  dB and  $\sigma_s = 0.01$  m. From this figure, it is evident that the effect of humidity on the ergodic capacity depends on the operation frequency. In more detail, we observe that up to 320 GHz the effect of relative humidity alteration is relatively low, whereas in the 380 GHz region, it is detrimental. For example, in 300 GHz, a relative humidity alteration from 30% to 70% results to a 0.03% ergodic capacity degradation, whereas the same alteration in the 380 GHz causes a corresponding 9.7% decrease. This indicates the importance of taking into account the variation of the environmental conditions in a geographical area, when selecting the operation frequency.

Fig. 4 illustrates the ergodic capacity as function of frequency and distance, assuming  $\frac{P}{N_o} = 25$  dB and  $\sigma_s = 0.01$  m. For a given operation frequency, as the distance

<sup>1</sup>According to [39] and [40], this antenna gain can be practically achieved by employing high-gain Cassegrain antennas.



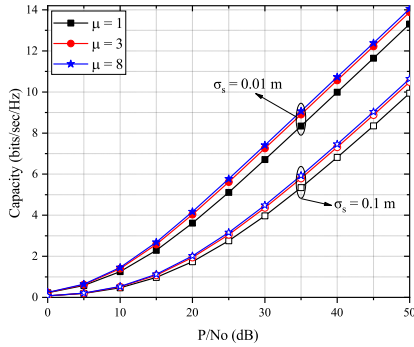


Fig. 5: Capacity vs  $\frac{P}{N_o}$  for different values of  $\mu$  and  $\sigma_s$ , for  $f = 275$  GHz and  $d = 40$  m.

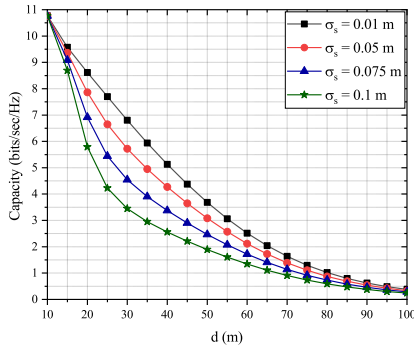


Fig. 6: Capacity vs distance for different values of  $\sigma_s$ ,  $f = 300$  GHz and  $\frac{P}{N_o} = 25$  dB.

increases the total path-loss also increases; hence, the ergodic capacity significantly decreases. Furthermore, for a fixed transmission distance, as the frequency increases, the path-loss drastically increases; hence, the ergodic capacity detrimentally decreases. For example, for  $f = 340$  GHz increasing the transmission distance from 20 m to 60 m causes an ergodic capacity degradation of approximately 78.6%. Similarly, for  $d = 20$  m and a frequency alteration from 300 GHz to 400 GHz results to an ergodic capacity decrease by about 15.7%.

Fig. 5 depicts the ergodic capacity as a function of  $\frac{P}{N_o}$ , for different values of  $\mu$  and  $\sigma_s$ , assuming  $f = 275$  GHz and  $d = 40$  m. The markers and lines indicate the fading parameter  $\mu$ , specifically the black ones stand for  $\mu = 1$ , the red ones for  $\mu = 3$  and the blue ones for  $\mu = 8$ . Also, the color filled markers denote the ergodic capacity calculated with  $\sigma_s = 0.01$  m, while the non-filled markers represent the results with  $\sigma_s = 0.1$  m. Note that the ergodic capacity of the Rayleigh multipath fading ( $\mu = 1$ ) is provided in this figure to serve as benchmark for the worst case scenario. For a given  $\frac{P}{N_o}$  and  $\sigma_s$ , as the fading parameter  $\mu$  increases the effect multipath fading decreases; therefore, the overall SNR improves yielding greater capacity. For example, for  $\frac{P}{N_o} = 40$  dB and  $\sigma_s = 0.01$  m changing  $\mu$  from 1 to 3 and from 1 to 8, causes a 5.8% and 7.4% ergodic

capacity increase, respectively, while for the same  $\frac{P}{N_o}$  and  $\sigma_s = 0.1$  m, the same  $\mu$  alterations lead to an ergodic capacity increase of 7.3% and 9.5%, respectively. Furthermore, for a given  $\frac{P}{N_o}$  and  $\mu$ , the increase of jitter variance significantly deteriorates the achievable ergodic capacity. For instance, for  $\frac{P}{N_o} = 30$  dB and  $\mu = 3$ , the increase of  $\sigma_s$  from 0.01 m to 0.1 m results to an ergodic capacity degradation of 40%. Finally, this figure reveals that the impact of misalignment fading is somewhat more detrimental compared to the one of multipath fading.

Fig. 6 presents the ergodic capacity as a function of the transmission distance, for different values of  $\sigma_s$ , assuming  $\frac{P}{N_o} = 25$  dB and  $f = 300$  GHz. As expected, for a given  $\sigma_s$ , the increase of the transmission distance causes detrimental increase of the path-loss; as a consequence, the achievable ergodic capacity severely degrades. For example, for  $\sigma_s = 0.05$  m, a transmission distance change from 20 m to 50 m reduces the achieved ergodic capacity by 60.8%. Furthermore, for a fixed transmission distance, the increase of  $\sigma_s$  drastically deteriorates the ergodic capacity. For instance, for  $d = 40$  m, a  $\sigma_s$  alteration from 0.01 m to 0.05 m, and 0.1 m results to an ergodic capacity degradation of 16.8%, while a  $\sigma_s$  change from 0.01 m to 0.075 m in a 34.2% ergodic capacity degradation. This indicates the importance of taking into account the level of antennas' misalignment, when evaluating the ergodic capacity performance of the THz wireless fiber extender.

## V. CONCLUSIONS

We studied the performance of wireless THz fiber extenders, when the transceivers antennas are not fully-aligned. In particular, by assuming  $\alpha - \mu$  fading and Gaussian distributions for the elevation and horizontal displacement, we provided the analytical framework for evaluating the ergodic capacity. Our results illustrated the degradation due to the effect of misalignment fading on the ergodic capacity of the THz wireless fiber extender. It was also revealed that the impact of misalignment fading is somewhat more detrimental compared to the one of the multipath fading. Finally, the importance of accurate misalignment characterization in the realistic performance analysis and design of THz wireless fiber extenders was highlighted.

## REFERENCES

- [1] A.-A. A. Boulogeorgos, E. N. Papatotiriou, and A. Alexiou, "Analytical performance assessment of THz wireless systems," *IEEE Access*, vol. 7, no. 1, pp. 1–18, Jan. 2019.
- [2] A.-A. A. Boulogeorgos, A. Alexiou, T. Merkle, C. Schubert, R. Elschner, A. Katsiotis, P. Stavrianos, D. Kritharidis, P. K. Chartsias, J. Kokkonen, M. Juntti, J. Lehtomäki, A. Teixeira, and F. Rodrigues, "Terahertz technologies to deliver optical network quality of experience in wireless systems beyond 5G," *IEEE Commun. Mag.*, vol. 56, no. 6, pp. 144–151, Jun. 2018.
- [3] I. F. Akyildiz, J. M. Jornet, and C. Han, "Terahertz band: Next frontier for wireless communications," *Phys. Commun.*, vol. 12, pp. 16–32, Sep. 2014.

- [4] A.-A. A. Boulogeorgos, A. Alexiou, D. Kritharidis, A. Katsiotis, G. Ntouni, J. Kokkonemi, J. Lehtomäki, M. Juntti, D. Yankova, A. Mokhtar, J.-C. Point, J. Machodo, R. Elschner, C. Schubert, T. Merkle, R. Ferreira, F. Rodrigues, and J. Lima, "Wireless terahertz system architectures for networks beyond 5G," TER-RANOVA CONSORTIUM, White paper 1.0, Jul. 2018.
- [5] A.-A. A. Boulogeorgos, E. N. Papatotiriou, J. Kokkonemi, J. Lehtomäki, A. Alexiou, and M. Juntti, "Performance evaluation of THz wireless systems operating in 275-400 GHz band," *IEEE Vehicular Technology Conference (VTC)*, 2018.
- [6] A.-A. A. Boulogeorgos, S. Goudos, and A. Alexiou, "Users association in ultra dense THz networks," in *IEEE International Workshop on Signal Processing Advances in Wireless Communications (SPAWC)*, Kalamata, Greece, Jun. 2018.
- [7] A.-A. A. Boulogeorgos, E. Papatotiriou, and A. Alexiou, "A distance and bandwidth dependent adaptive modulation scheme for THz communications," in *19th IEEE International Workshop on Signal Processing Advances in Wireless Communications (SPAWC)*, Kalamata, Greece, Jul. 2018.
- [8] C. Han and Y. Chen, "Propagation modeling for wireless communications in the terahertz band," *IEEE Commun. Mag.*, vol. 56, no. 6, pp. 96–101, Jun. 2018.
- [9] G. A. Siles, J. M. Riera, and P. G. del Pino, "Atmospheric attenuation in wireless communication systems at millimeter and THz frequencies [wireless corner]," *IEEE Antennas Propag. Mag.*, vol. 57, no. 1, pp. 48–61, Feb. 2015.
- [10] P. Boronin, V. Petrov, D. Moltchanov, Y. Koucheryavy, and J. M. Jornet, "Capacity and throughput analysis of nanoscale machine communication through transparency windows in the terahertz band," *Nano Commun. Networks*, vol. 5, no. 3, pp. 72–82, Sep. 2014.
- [11] C. Lin and G. Y. L. Li, "Terahertz communications: An array-of-subarrays solution," *IEEE Commun. Mag.*, vol. 54, no. 12, pp. 124–131, Dec. 2016.
- [12] N. Akkari, J. M. Jornet, P. Wang, E. Fadel, L. Elrefaie, M. G. A. Malik, S. Almasri, and I. F. Akyildiz, "Joint physical and link layer error control analysis for nanonetworks in the terahertz band," *Wireless Networks*, vol. 22, no. 4, pp. 1221–1233, May 2016.
- [13] S. Han, C. I. I. Z. Xu, and C. Rowell, "Large-scale antenna systems with hybrid analog and digital beamforming for millimeter wave 5G," *IEEE Commun. Mag.*, vol. 53, no. 1, pp. 186–194, Jan. 2015.
- [14] J. M. Jornet and I. F. Akyildiz, "Channel modeling and capacity analysis for electromagnetic wireless nanonetworks in the terahertz band," *IEEE Trans. Wireless Commun.*, vol. 10, no. 10, pp. 3211–3221, Oct. 2011.
- [15] J. Kokkonemi, J. Lehtomäki, and M. Juntti, "Simplified molecular absorption loss model for 275-400 gigahertz frequency band," in *12th European Conference on Antennas and Propagation (EuCAP)*, London, UK, Apr. 2018.
- [16] E. N. Papatotiriou, J. Kokkonemi, A.-A. A. Boulogeorgos, J. Lehtomäki, A. Alexiou, and M. Juntti, "A new look to 275 to 400 GHz band: Channel model and performance evaluation," in *IEEE International Symposium on Personal, Indoor and Mobile Radio Communications (PIMRC)*, Bologna, Italy, Sep. 2018.
- [17] H. Elayan, R. M. Shubair, J. M. Jornet, and P. Johari, "Terahertz channel model and link budget analysis for intrabody nanoscale communication," *IEEE Trans. Nanobioscience*, vol. 16, no. 6, pp. 491–503, Sep. 2017.
- [18] M. A. Akkas, "Terahertz channel modelling of wireless ultra-compact sensor networks using electromagnetic waves," *IET Commun.*, vol. 10, no. 13, pp. 1665–1672, 2016.
- [19] C. Han, A. O. Bicen, and I. F. Akyildiz, "Multi-ray channel modeling and wideband characterization for wireless communications in the terahertz band," *IEEE Trans. Wireless Commun.*, vol. 14, no. 5, pp. 2402–2412, May 2015.
- [20] J. Kokkonemi, J. Lehtomäki, and M. Juntti, "Frequency domain scattering loss in THz band," in *Global Symposium on Millimeter-Waves (GSMM)*, Montreal, Canada, May 2015, pp. 1–3.
- [21] A. R. Ekti, A. Boyaci, A. Alparslan, . Ünal, S. Yarkan, A. Grin, H. Arslan, and M. Uysal, "Statistical modeling of propagation channels for terahertz band," in *IEEE Conference on Standards for Communications and Networking (CSCN)*, Helsinki, Finland, Sep. 2017, pp. 275–280.
- [22] S. Kim and A. Zajić, "Statistical modeling and simulation of short-range device-to-device communication channels at sub-THz frequencies," *IEEE Trans. Wireless Commun.*, vol. 15, no. 9, pp. 6423–6433, Sep. 2016.
- [23] S. Priebe, M. Jacob, and T. Kürner, "The impact of antenna directivities on THz indoor channel characteristics," in *6th European Conference on Antennas and Propagation (EuCAP)*, Prague, Czech Republic, Mar. 2012, pp. 478–482.
- [24] A. Afsharinejad, A. Davy, B. Jennings, S. Rasmann, and C. Brennan, "A path-loss model incorporating shadowing for THz band propagation in vegetation," in *IEEE Global Communications Conference (GLOBECOM)*, San Diego, CA, USA, Dec. 2015, pp. 1–6.
- [25] C. Han and I. F. Akyildiz, "Three-dimensional end-to-end modeling and analysis for graphene-enabled terahertz band communications," *IEEE Trans. Veh. Technol.*, vol. 66, no. 7, pp. 5626–5634, Jul. 2017.
- [26] C. Liu, Y. Yao, Y. Sun, and X. Zhao, "Average capacity for heterodyne FSO communication systems over gamma-gamma turbulence channels with pointing errors," *Electron. Lett.*, vol. 46, no. 12, pp. 851–853, Jun. 2010.
- [27] I. S. Gradshteyn and I. M. Ryzhik, *Table of Integrals, Series, and Products*, 6th ed. New York: Academic, 2000.
- [28] M. Abramowitz and I. A. Stegun, *Handbook of Mathematical Functions with Formulas, Graphs, and Mathematical Tables*, 9th ed. New York: Dover Publications, 1972.
- [29] A. P. Prudnikov, Y. A. Brychkov, and O. I. Marichev, *Integral and Series: Volume 3, More Special Functions*. CRC Press Inc., 1990.
- [30] A. A. Farid and S. Hranilovic, "Outage capacity optimization for free-space optical links with pointing errors," *Journal of Lightwave Technology*, vol. 25, no. 7, pp. 1702–1710, Jul. 2007.
- [31] S. Arnon, "Effects of atmospheric turbulence and building sway on optical wireless-communication systems," *Opt. Lett.*, vol. 28, no. 2, pp. 129–131, Jan. 2003.
- [32] H. G. Sandalidis, T. A. Tsiftsis, and G. K. Karagiannidis, "Optical wireless communications with heterodyne detection over turbulence channels with pointing errors," *Journal of Lightwave Technology*, vol. 27, no. 20, pp. 4440–4445, Oct. 2009.
- [33] L. Yang, X. Gao, and M.-S. Alouini, "Performance analysis of relay-assisted all-optical FSO networks over strong atmospheric turbulence channels with pointing errors," *J. Lightwave Technol.*, vol. 32, no. 23, pp. 4011–4018, Dec. 2014.
- [34] M. D. Yacoub, "The  $\alpha - \mu$  distribution: A physical fading model for the stacy distribution," *IEEE Transactions on Vehicular Technology*, vol. 56, no. 1, pp. 27–34, Jan 2007.
- [35] H. Lei, C. Gao, Y. Guo, and G. Pan, "On physical layer security over generalized gamma fading channels," *IEEE Commun. Lett.*, vol. 19, no. 7, pp. 1257–1260, Jul. 2015.
- [36] A. Papoulis and S. Pillai, *Probability, Random Variables, and Stochastic Processes*, ser. McGraw-Hill series in electrical engineering: Communications and signal processing. Tata McGraw-Hill, 2002.
- [37] V. S. Adamchik and O. I. Marichev, "The algorithm for calculating integrals of hypergeometric type functions and its realization in REDUCE system," in *Proceedings of the international symposium on Symbolic and algebraic computation (ISSAC)*. Tokyo, Japan: ACM, Aug. 1990, pp. 212–224.
- [38] "The wolfram functions site," <http://functions.wolfram.com/07.34.21.0012.01>, accessed: 2018-08-08.
- [39] S. Koenig, D. Lopez-Diaz, J. Antes, F. Boes, R. Henneberger, A. Leuther, A. Tessmann, R. Schmogrow, D. Hillerkuss, R. Palmer, T. Zwick, C. Koos, W. Freude, O. Ambacher, J. Leuthold, and I. Kallfass, "Wireless sub-THz communication system with high data rate," *Nat. Photonics*, vol. 7, pp. 977 EP–, Oct. 2013.
- [40] K. Guan, G. Li, T. Krner, A. F. Molisch, B. Peng, R. He, B. Hui, J. Kim, and Z. Zhong, "On millimeter wave and THz mobile radio channel for smart rail mobility," *IEEE Trans. Veh. Technol.*, vol. 66, no. 7, pp. 5658–5674, Jul. 2017.